Chapter 1

Introduction

Acceleration of particles and the consequent transport and radiation effects are ubiquitous in astrophysical plasmas, such as those responsible for cosmic ray particles, gamma-ray bursts, and flares on accretion disks near compact objects (e.g., black holes and X-ray binaries). Solar flares serve as one of the most suitable laboratories to study particle acceleration and related high-energy processes, because of the proximity of the Sun and abundant observations available. The primary goal of this research is to understand particle acceleration mechanisms in general, and how these mechanisms operate in solar flares in particular.

1.1 Solar Flare Observations and Models

Solar flares are one of the two most energetic phenomena on the Sun (the other being coronal mass ejections, CMEs), involving up to some 10^{32} ergs or more energy released on a timescale of a few minutes to tens of minutes (cf., solar luminosity of 3.8×10^{33} ergs s^{-1}). The first flare ever observed was an emission burst in white-light discovered on 1859 September 01 by R. C. Carrington and R. Hodgson independently. Since then, flare observations have been accumulated over a century in many other wavelengths, including Hα, radio waves, as well as X-rays and gamma-rays in recent decades.

Theoretical investigations of solar flares have lagged behind. Among the earliest flare models were those proposed by Carmichael (1964), Sturrock (1966), Hirayama (1974), and Kopp & Pneuman (1976). These 2-D models, in one way or another, involve magnetic reconnection (Sweet, 1958; Parker, 1963; Petschek, 1964) with an inverted "Y"- or an "X"-shaped topology, in a (vertical) current sheet, which can be produced by a preceding CME or magnetic flux emergence from below the photosphere. Advances in recent decades have improved on these early models, but the basic picture remains the same.

In the currently widely accepted scenario, the basic physical processes involved and the observational signatures are as follows. Magnetic reconnection, as the primary energy release mechanism occurring in the corona, leads to plasma heating and particle acceleration. Some particles escape along the open magnetic field lines into the interplanetary space, with electrons producing various radio bursts and some electrons (Wang et al., 2006; Krucker et al., 2007) and ions (Krucker & Lin, 2000) being detected at 1 AU. Other particles escape along the newly reconnected closed magnetic loop to lower layers of the atmosphere.

Electrons, while spiraling along magnetic field lines, can produce microwave bursts via synchrotron radiation. These electrons, in the meanwhile, lose their energy through Coulomb collisions with the ambient plasma, primarily in the transition region and chromosphere where the density is sufficiently high, and produce *thick-target* (Brown, 1971; Petrosian, 1973) hard X-rays (HXRs) via bremsstrahlung. This results in the so-called footpoint (FPs; Hoyng et al., 1981; Sakao, 1994; Petrosian et al., 2002) emission observed at HXR energies. Accelerated ions, while colliding with background particles, can excite nuclear reactions and produce gamma-ray emission (e.g., Ramaty & Murphy, 1987; Hurford et al., 2003).

The released energy, which is carried by particles and/or thermal conduction and transferred to lower atmospheres, can heat the chromosphere rapidly. The resulting overpressure in the over-heated chromosphere can drive a mass flow upward along the loop at a speed of a few hundred km s^{-1}, which can be observed as blue-shifted chromospheric emission lines. The mass motion fills the flaring loop with a hot plasma, giving rise to the loop structure seen in soft X-ray (SXR) and gradual evolution of SXR flux. This process, termed *chromospheric evaporation* by Neupert (1968), was proposed to explain the empirical temporal relationship of the derivative of the SXR flux and the microwave or HXR light curve, i.e., the Neupert effect (Hudson, 1991), which is observed in some (but not all) flares (Dennis & Zarro, 1993).

Consequent energy redistribution in the lower layers of the atmosphere, on the other hand, can produce ribbons seen in Hα and occasionally in white-light (e.g., Hudson et al., 2006) for the brightest flares. As time proceeds, reconnection develops to higher altitudes in the inverted-Y shaped configuration, and the two HXR FPs and Hα ribbons are usually seen move away from each other, in a direction more or less perpendicular to the magnetic neutral line. This gives the standard picture of a two-ribbon flare.

1.2 Stochastic Particle Acceleration Model

There are two most important unresolved questions regarding the physics of solar flares. The first is how energy is released, which involves details of the magnetic reconnection process. The other is how particles are accelerated, which is the main goal of this book, and we focus on acceleration of electrons here.

In general, there are three types of acceleration commonly quoted for solar flares (and other astrophysical plasmas). (1) **Direct electric field acceleration** (e.g., Holman, 1985; Benka & Holman, 1994) can boost a particle to high energies simply via the Coulomb force from the electric field and may operate in the current sheet or in the reconnection site, but it is difficult to maintain a large-scale coherent DC electric field. (2) **Shock or first-order Fermi acceleration** (e.g., Tsuneta & Naito, 1998) can energize particles by making them repeatedly pass through the shock front back and forth and this mechanism may be present in the fast shock produced by the super-magnetosonic outflow jet from the reconnection region. However, it would be difficult to reflect the particles in the upstream region. (3) **Stochastic (second-order Fermi) acceleration** by turbulence or plasma waves is the most likely mechanism for solar flares (Petrosian, 1994, 1996), compared with the shortcomings of the other two mechanisms (although they may also be operating to some extent).

The **stochastic acceleration (SA)** mechanism has been studied and advanced by many authors for solar flares with various purposes (e.g. Ramaty, 1979; Ramaty & Murphy, 1987; Hamilton & Petrosian, 1992; Miller et al., 1996; Park et al., 1997; Petrosian & Liu, 2004), and for astrophysical environments (e.g., around black holes, Liu et al., 2004b, 2006b). The SA model is supported by remote HXR observations and by *in situ* measurements of interplanetary particles. In particular, Liu, Petrosian, & Mason (2004a, 2006c) have shown that the enhanced ^{3}He over ^{4}He ions observed by the *Advanced Composition Explorer* (*ACE*) spacecraft can be accounted for by the preferential resonance interactions of ^{3}He with turbulence.

In the SA model, the basic picture is as follows (see Fig. 1.1, *left panel*). As a consequence of magnetic reconnection, large-scale turbulence or plasma waves are generated at/near the reconnection region. Turbulence then cascades to small scales, and accelerates particles and heats the plasma via resonance wave-particle interactions in a region near/at the top of the flaring loop. The accelerated particles produce in the acceleration region the *thin-target* HXR loop-top (LT) source (Masuda 1994), which was one of the major discoveries of the *Yohkoh* mission. Some particles are trapped in the acceleration region due to scattering by turbulence, some escape down to lower atmospheres to produce the *thick-target* FP emission, and others escape up into interplanetary space along open field lines as mentioned above.

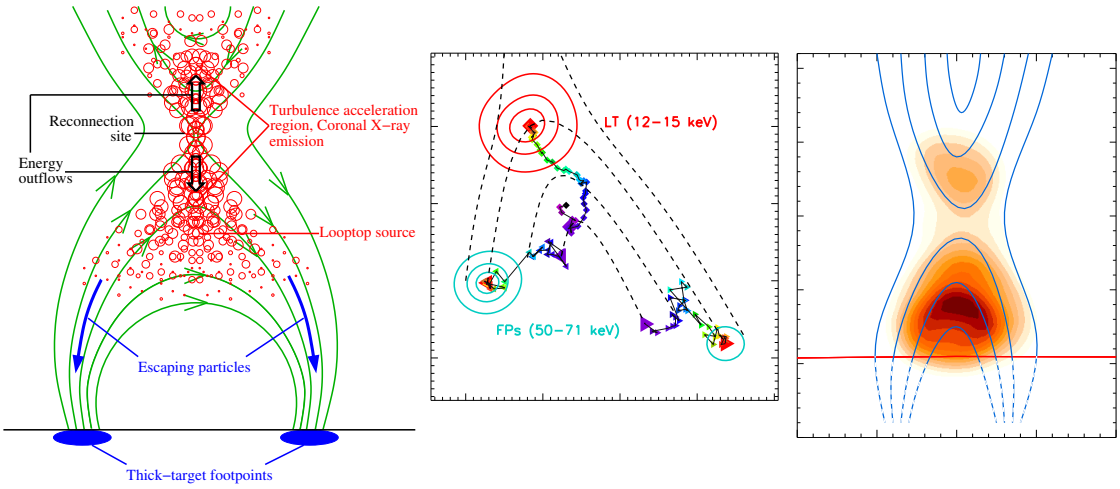

Figure 1.1: *Left:* Sketch of the stochastic acceleration model (Hamilton & Petrosian, 1992; Park & Petrosian, 1995; Petrosian & Liu, 2004) proposed for solar flares. The curves are magnetic field lines in a possible configuration; the open circles represent turbulence or plasma waves that are generated during magnetic reconnection. *Middle:* Temporal evolution of the LT and FP HXR sources of the 2003 November 03 X10 flare (see Chapter 3). The symbols indicate the source centroids and the gray scale from dark to bright shows time at 20 s intervals, with contours for the last interval. The dashed curves connect schematically the FP and LT sources for different times showing the expected evolution for the model on the left. *Right:* Image of the 2002 April 30 M1.4 flare (see Chapter 4), showing an elongated LT source with two distinct peaks as expected from the model on the left. The horizontal line indicates the solar limb which occulted the FPs and the curves (added by hand) represent the magnetic field lines. Both the middle and right panels are rotated from their original orientations for ease of viewing.

The stochastic acceleration process can be described by the Fokker-Planck equation,

$$\frac{\partial f}{\partial t} = \frac{\partial}{\partial E}\left[D(E)\frac{\partial f}{\partial E}\right] + \frac{\partial}{\partial E}\{[A(E) - \dot{E}_L]f\} - \frac{f}{T_{\rm esc}(E)} + Q(E)\,, \tag{1.1}$$

where $f \equiv f(t, E)$ is the electron distribution function, $E = \gamma - 1$ (γ being the Lorentz factor) is the electron kinetic energy in units of $m_e c^2$, $D(E)$ and $A(E)$ are the energy diffusion and systematic acceleration coefficients, $T_{\rm esc}$ is the particle escape time, $Q(E)$ is the total injection flux of electrons into the acceleration region that acts as source term in the equation. $\dot{E}_L = \dot{E}_{\rm Coul} + \dot{E}_{\rm synch}$ is the absolute value of the net systematic energy loss rate, which is a combination of Coulomb loss $\dot{E}_{\rm Coul}$ and synchrotron loss $\dot{E}_{\rm synch}$. The central task of such a model is to determine the resonance condition for a particle (with a given momentum and pitch angle) and a given turbulence spectrum, and thus obtain the coefficients $D(E)$, $A(E)$, and $T_{\rm esc}$.

The subsequent particle transport in the flare loop can be described with a similar diffusion equation, with the addition of the magnetic mirroring effect and pitch angle scattering. A unified code, called *$\mathcal{F}$lare*, that can calculate the particle acceleration and transport, together with bremsstrahlung radiation, has been developed (Petrosian, Donaghy, & Llyod 2001), on the basis of previous advances accumulated over two decades (Leach, 1984; McTiernan, 1989; Lu, 1989; Hamilton, 1990; Park, 1996). This code was used in the theoretical modeling part of this book (see Chapter 7).

1.3 Hard X-ray Observations and *RHESSI* Instruments

HXRs (and gamma-rays) observed during the impulsive phase of flares provide the most direct information on the spectrum of accelerated particles and give us clues to the acceleration mechanisms. A power-law distribution (with an index of δ) of electrons, for example, can produce a power-law HXR spectrum with a photon index of $\gamma \simeq \delta \pm 1$ from a thin- and thick-target sources, respectively.

Observations by HXR instruments on board earlier missions,[1] including *Orbiting Solar Observatory-5* and -7, *International Sun-Earth Explorer* (*ISEE*)-3, *Solar Maximum Mission* (*SMM*), *Hinotori*, *Compton Gamma Ray Observatory* (*CGRO*), and *Yohkoh*, have advanced our understanding on this subject (see the review by Aschwanden, 2004). The currently active *Reuven Ramaty High Energy Solar Spectroscopic Imager* (*RHESSI*) mission with its superior capabilities (Lin et al., 2002) has proven that it can make a more accurate determination of temporal, spectral and spatial evolution of flares (see the *RHESSI* dedicated *Solar Physics* Vol. 210, 2002 and *Astrophysical Journal Letters* Vol. 595, No. 2, 2003).

RHESSI is a NASA small explorer (SMEX) mission, designed to study particle acceleration and energy release in solar flares (and some non-solar science, Lin et al. 2002). It has an array of nine large-volume (300 $\rm cm^3$) coaxial germanium detectors (Smith et al., 2002), with a total collecting area of $\sim 150\,\rm cm^2$. This provides an energy resolution down to $\sim 1\,$keV and an energy coverage of 3 keV–17 MeV. Its imaging capability is enabled by the Rotating Modulation Collimator (RMC) system and the spacecraft spin at 15 rpm ($\sim 4\,$s period). Each of the nine subcollimators consists of two grids, 1.55 m apart, with the

[1] See Aschwanden (2004, p. 552) for a complete list of previous HXR instruments.

germanium detector equipped behind the rear grid. During a flare, each photon arriving at the detector is tagged with its arrival time and energy. Then the spatial information is recovered through the image reconstruction procedure at the time of data analysis on the ground, which is realized by Fourier transform of the time series data of energy tagged counts, i.e., the modulation pattern (Hurford et al., 2002). Such a unique imaging system produces an angular resolution of $2.3''$ in its 1° field of view (covering the full Sun). The temporal resolution can reach $\sim 2\,\mathrm{s}$ for detailed images and tens of ms for basic images.

Since its launch, *RHESSI* has provided us with unprecedented details of solar flares, some of which are serendipitous (e.g., Liu, W. et al., 2006) and some of which pose new challenges to theoretical models (e.g., Sui & Holman, 2003; Hurford et al., 2003). We will present some of such observations in this book.

1.4 Introduction to This Book

The main theme of this book is the investigation of the micro and macro physics of the acceleration and transport of particles (electrons[2]) in solar flares, and their thermal and nonthermal radiative signatures. To reach this objective, we took a two-prong attack, using HXR data analysis and theoretical modeling, both couched in the framework of the SA model. Our data analysis concentrated on HXR images and spectra observed by *RHESSI* during the impulsive phase of flares. Our modeling efforts was devoted to combining the SA model and the *Flare* code with a hydrodynamic (HD) model (Mariska, Emslie, & Li, 1989) to study the interplay of the particle acceleration, transport, and radiation effects and the atmospheric response to the energy deposition by accelerated electrons.

1.4.1 *RHESSI* Observations

During 1970s and 1980s, HXR imagers on board early missions, such as *SMM* and *Hinotori*, revealed the FP emission which supports the thick-target model (Brown, 1971; Petrosian, 1973) for solar flares. In early 1990s, the *Yohkoh* mission discovered the HXR LT source (Sakao, 1994; Masuda, 1994), which marked a milestone in flare research and provided further evidence for the stochastic acceleration model (e.g., Hamilton & Petrosian, 1992). *RHESSI*, with its superior capabilities, can provide more accurate temporal, spatial, and spectral information of the LT and FP (and other possible) sources and thus help improve theoretical models. Obtaining such information of individual sources and offering appropriate physical interpretations is the main task of the observational part of this book.

In the SA model, the LT emission comes directly from the accelerated electrons (thin target) and the FP emission is produced by escaping electrons in a thick target region. The fluxes and spectra of the two sources are related and can thus be used to constrain the SA model parameters. We have carried out a preliminary statistical study of 29 *limb* flares, which have minimal projection effects, and obtained the relative spectra and fluxes of the LT and FP sources. We find a large difference between the average values of the LT and FP spectral indexes, which, together with other statistical results, will be presented in *Chapter 2*. This statistical study have also paved the path to identify four interesting flares

[2] Acceleration of protons and other ions is another aspect of solar flare energetics, and is beyond the scope of this work.

for in-depth investigations, each of which presents *evidence* of particular aspects as well as imposes *challenges* for the classical reconnection model of solar flares.

In the classical flare model, as mentioned earlier, magnetic reconnection takes place at lower altitudes first and progresses to higher overlying loops as time proceeds. In this picture, one would expect that the FPs move apart while the LT source moves up with time. We will show in *Chapter 3* an excellent example (the 2003 November 03 X3.9 flare, see Fig. 1.1, *middle*) of such a picture. In the following two chapters, we will focus on the LT and the FP emission respectively.

In the common 2-D reconnection picture, outflow jets of high speed plasmas are present in opposite directions along the current sheet. Accelerated particles and heated plasmas are expected to be present in both directions as well. As we can see in Figure 1.1 (*right panel*), an M1.4 flare occurring on 2002 April 30 exhibits a double-source structure in the corona, which suggests that reconnection takes place in between. Analysis of the images and spectra of this flare will be presented in *Chapter 4*.

We now turn our attention from coronal (LT) emission to chromospheric (FP) emission. As noted earlier HXR observations can provide useful information about the electron spectrum, while magnetic field measurements of the flare region can give clues to magnetic reconnection development. Combining both observations, if available, can improve our understanding of flares. As we will see in *Chapter 5*, the 2003 October 29 X10 flare, which occurred near the disk center and thus had minimal projection effects for line-of-sight magnetic field measurement, provided us such an excellent opportunity.

In *Chapter 6*, we will, again, examine both LT and FP emissions. The 2003 November 13 M1.7 flare shows some unusual spatial evolution and provides direct evidence for chromospheric evaporation. We find that emission from the legs of the loop dominates at intermediate energies and the emission centroids move from the FPs to the LT as time proceeds. This suggests an increase of loop density, possibly as a consequence of chromospheric evaporation. However, some observed source morphologies and their evolution cannot be accounted for by previous modeling efforts. Therefore, simulations with more realistic physical conditions are required to explain the results as well as the particle acceleration & transport and plasma heating processes.

1.4.2 Combining the Fokker-Planck and Hydrodynamic Codes

Motivated by the *RHESSI* observations mentioned above, we have embarked on an investigation of combining the Fokker-Planck $\mathcal{F}$*lare* code with the Naval Research Laboratory (NRL) flux tube hydrodynamic (HD) model (Mariska, Emslie, & Li 1989). Aside from the observational incentive, the theoretical motivation comes as follows.

There are basically two faces of a solar flare — one concerns energetic particles and their transport and radiation effects, and the other concerns the hydrodynamic evolution of the plasma in the flare loop. These two aspects are actually coupled together in a circular chain. Particles, on the one hand, lose their energy via Coulomb collisions and heat the background plasma, which causes chromospheric evaporation that changes the density and temperature distribution in the loop. In turn, such changes affect the particle acceleration and transport processes and influence the spectrum of the accelerated particles. The energy deposition rate (by particles) will also be altered and fed back to the hydrodynamics of the

background plasma.

Due to the complexity of the subject, however, people tend to decouple these processes and study one at a time while assuming some simple forms for the others. For particle acceleration and transport, as mentioned earlier, one of the main streams of studies solves the Fokker-Planck equation and keeps track of the particle distribution function (e.g., Leach 1984; McTiernan 1989), assuming a *static* background atmosphere. For the hydrodynamics, a majority of efforts (e.g., Fisher et al., 1985c,b) are put into 1-D numerical HD simulations, assuming the plasma can only move along the magnetic field line, which is a valid assumption for a magnetic field dominated (low-β) plasma. In such simulations, some form of a *simple* (e.g., power-law) electron distribution is usually assumed and results from simplified analytical solutions are used to provide the heating rate.

A more realistic and self-contained treatment of both particles and gas dynamics is thus desired. We have started such an investigation and engineered the two codes (as mentioned above) to work together, which possesses the potential to advance our understanding of solar flares significantly. We have used the newly combined code to examine the atmospheric response to the energy deposition of electrons with a spectrum predicted by the SA model (Petrosian & Liu, 2004). Our approach and result will be presented in *Chapter 7*.

From the same simulations, we have also examined the empirical Neupert effect with more rigorous (than previous works, e.g., by Veronig et al. 2005) calculations of the energy contents and thermal and nonthermal X-ray radiation. This study will be presented in *Chapter 8*.

As an extension of our studies on the flare impulsive phase, we will present in *Chapter 9* a simulation of the decay phase. The goal here is to test the effects of suppression of conduction and/or heating, presumably produced by turbulence (at a lower level during the decay phase), in the presence of HD *flows*. Our earlier analytical investigation (Jiang et al., 2006) of the problem assumed a hydrostatic atmosphere which is an approximation, and rigorously speaking, not quite realistic. Our result confirms the earlier conclusion that suppression of conduction and/or heating is required to explain the X-ray observations and suggests that an even larger factor of suppression would be needed.

Finally, in *Appendixes A–C*, we will provide a comprehensive description of the *RHESSI* data analysis procedures employed here, an account of the techniques used for analyzing HXR FP asymmetries, and a note on the improvement of the current SA model by inclusion of Coulomb collisions with a warm/hot background plasma.